Chemical heterogeneities in tungsten containing TiAl alloys processed by powder metallurgy

Alain Couret, Melissa Allen, Marcus Willi Rackel, Benjamin Galy, Jean-Philippe Monchoux, Volker Güther, Florian Pyczak, Pierre Sallot, Marc Thomas

Chemical heterogeneities in tungsten containing TiAl alloys processed by powder metallurgy

Alain Couret [1], Melissa Allen [2], Marcus Willi Rackel [3], Benjamin Galy [1], Jean-Philippe Monchoux [1], Volker Güther [2], Florian Pyczak [3], Pierre Sallot [4] and Marc Thomas [5]

1. CEMES, Université de Toulouse, CNRS, 29 rue Jeanne Marvig, BP 94347, 31055 Toulouse, France
2. GfE Metalle and Materialien GmbH, Höfener Straβe 45, Nürnberg, Germany
3. Helmholtz-Zentrum Geesthacht, Institute for Materials Research, D-21502 Gesthacht, Germany
4. Safran Tech, Materials and Processes, Rue des Jeunes Bois, Ch^ateaufort, 78114, Magny-Les-Hameaux, France
5. ONERA/DMAS Université Paris Saclay, 29 Avenue de la Division Leclerc, BP 72, 92322 Châtillon Cedex, France

* Corresponding author: alain.couret@cemes.fr

Abstract

During the last decade, it has been shown that the W-containing IRIS-TiAl alloy displays promising properties for structural applications at high temperatures. The manufacturing process of this alloy is divided into three successive steps: electrode production, powder atomisation and spark plasma sintering (SPS) densification. However, an IRIS alloy densified by using pre-alloyed powders atomized by EIGA process (Electrode Induction melting Gas Atomisation) has recently been found to exhibit chemical heterogeneities. The aim of the present work is to look for the origin of such heterogeneities all along this manufacturing process. The microstructures and the chemical compositions of the material obtained after these different steps are thus investigated at intermediate and local scales by using various experimental tools. A particular attention is paid to the distribution of tungsten atoms in correlation to the constituent phases. Effects of these heterogeneities on mechanical properties

are measured by performing tensile tests at room and high temperatures. It will be demonstrated that these heterogeneities are issued from tungsten segregation occurring during the first stage of the initial solidification of the electrode, thus prior to atomisation.

Keywords

Titanium aluminides; Powder atomisation; Spark Plasma Sintering; Tungsten segregation; Microstructure.

1. Introduction

During the last two decades, a number of investigations have demonstrated the interest of innovative powder metallurgy (PM) routes, such as Spark Plasma Sintering (SPS) or Additive Layer Manufacturing (ALM), to produce high quality TiAl alloys and/or sound components. Indeed, PM processing is generally known to result in grain size refinement as compared to cast processing, thus yielding significant strengthening for the considered alloys. However, at service temperatures, PM products can suffer from high creep rates in γ-TiAl alloys. In order to achieve a proper balance in mechanical properties, extensive work has been focused on alloy development, in particular with the addition of refractory elements such as niobium, molybdenum, tungsten, rhenium and tantalum.

Thence, the incorporation of these refractory elements, which promotes solidification by the β route, has emerged as an indispensable way of improving TiAl alloys to reach service temperatures superior to 700°C [1]. In particular, the as-SPS IRIS alloy ($Ti_{49.9}Al_{48.0}W_{2.0}B_{0.1}$, composition in at.%) has been found to possess promising mechanical properties at high temperatures combined with a reasonable ductility at room temperature [2,3]. The W addition was found to enhance mechanical properties through solid solution strengthening. Tungsten is also beneficial in terms of oxidation resistance [4]. Moreover, its low diffusion rate within the microstructure can guarantee an increased thermal stability at service temperatures for this family of W-bearing TiAl alloys [5]. The originality of this alloy lies in the addition of only 2 at.% of W due to its very low diffusivity, which makes it possible to maintain a high Al content (47-48 at. %). Thus, the presence of β_0 phase in the final microstructure, which is unfavourable at high temperatures and brittle at room temperature, is avoided while the presence of γ phase is promoted. The challenge is to have a homogeneous distribution of W atoms in the γ phase to ensure a homogeneous structural hardening of that phase and the alloy

via the interaction of W atoms with dislocations moving by various deformation mechanisms [6].

One of the outstanding features of the SPS process lies in the homogeneous and texture-free microstructures, after densification. Moreover, the process is fast enough to prevent grain growth or long range migration of atomic species. In this alloy development work, pre-alloyed powders, i.e. with the expected chemical composition of the alloy, have been used.

A first batch of powder was supplied by CRUCIBLE/ATI companies (Pittsburgh, PA, USA) [7] using the TGA technique (Titanium Gas Atomisation). More generally, TGA, as well as PIGA (Plasma Melting Induction Guiding Gas Atomization - [8]) and VIGA (Vacuum Inert Gas Atomisation - [9]), belong to the group of cold mould techniques [1]. In this case, the alloy is fully melted, guided into the centre of a nozzle and then atomised with a stream of high pressure inert gas. The powder particles are very rapidly solidified from the homogeneous melt bath. Fig. 1a shows the microstructure at a low magnification of an IRIS alloy obtained after densification of this CRUCIBLE/ATI TGA powder, using a conventional SPS cycle with a dwell temperature of 1350°C. Some dark circular areas coming from powder particles that are depleted in heavy elements, can be observed in Fig. 1a.

The main alternative route to produce pre-alloyed TiAl powders is by using the crucible-free technique called EIGA (Electrode Induction melting Gas Atomisation – [8]). In this case, the starting material is a pre-alloyed electrode, the end of which is machined into a cone shape. A conical induction coil, having the same shape as the tip of the electrode, is used to melt down the electrode, which is rotated to homogenise the temperature field at its tip and is slowly lowered into the induction coil as the fusion starts. The distance between the induction coil and the melting electrode is controlled to be constant. Drops of molten metal are falling through the gas-atomisation nozzle and are subsequently atomised. The absence of any contamination by a crucible is one of the main reasons, together with a reduced electric power consumption, large

batches of powder capabilities and lower maintenance costs of the facility, why this process has attracted many industrial developments recently. Fig. 1b presents an IRIS TiAl alloy obtained after densification of an EIGA powder, using the same SPS parameters as for Fig. 1a. Some bright features can be seen, which reveal some microstructural and chemical heterogeneities.

The increasing propensity for structural heterogeneities in the EIGA-SPS-IRIS alloy compared to the TGA-SPS-IRIS one was unexpected since previous results with other TiAl alloys did show a rather robust EIGA procedure. For example, the EIGA-SPS route with the so-called GE composition (Ti-48Al-2Cr-2Nb) exhibited good homogeneity. In this context, the present authors have gathered their skills and means for further understanding and handling the problem of such structural heterogeneities in order to improve the EIGA production route applied to the IRIS alloy and, in a more general point of view, to TiAl alloys containing refractory elements.

2. Materials and methods

The IRIS alloys studied in this work were produced by a process in three successive steps: centrifugal casting of electrodes, powder atomisation and SPS densification.

Electrodes were produced at GfE-GmbH in three steps. More details about the GfE means and processes can be found in the paper of Güther *et al.* [10]. First, electrodes were uniaxially compacted using Ti sponges, Aluminium, WAl and AlB master alloys. Second, small sized ingots (7kg) were processed by single VAR (Vacuum Arc Remelting). Third, VAR ingots were remelted for homogenisation in an induction skull melter and then centrifugally casted in cylindrical steel moulds with a tip at the bottom end. With this process, several electrodes with a diameter of 50 mm, typically from seven to nine, can be casted in a single pour. The critical issues are the control of the alloy chemical composition including the impurity level, as well as the homogeneity of the ingot. Two sets of electrodes, called GFE1 and GFE2 in the following, were processed. Their average compositions are given in Table 1. The aluminium

contents are higher than scheduled due to a lower evaporation of this element than expected during the process. Aside from a 0.57at% difference in Al content, GFE2 mainly exhibits an extra 0.7at%Nb and a higher oxygen content with respect to GFE1. This excess in the oxygen content in GFE2 electrode is mainly due to the use of different master alloy batches.

Tab. 1. *Chemical compositions of the electrodes GFE1 and GFE2.*

	Ti	Al	W	B	Nb	Cu	Ni	Cr	Fe	Si	C	O	H	N
	Atomic %											ppm Weight		
GFE1	48.80	49.07	1.79	0.08	0	0.01	0.01	0.01	0.06	0.0.14	0.03	330	10	10
GFE2	48.46	48.50	1.79	0.07	0.73	0.01	0.01	0.01	0.04	0.27	0.11	1200	120	10

Electrodes of the two GFE1 and GFE2 compositions were atomized respectively at TLS Technik company (Bitterfeld –Wolfen, Germany) and Helmholtz-Zentrum Geesthacht (HZG, Geesthacht, Germany), by the EIGA process. At HZG,an electrode was atomised in six successive runs to get approximately powder batches representative of the material present around the locations L1 to L6 (Fig. 2). Two atomisation rates were alternatively used depending on the location: 16 kg/hour for locations L1, L3 and L5 and 45 kg/hour for L2, L4 and L6. Corresponding powder batches are denominated BS1, BR2, BS3, BR4, BS5 to BR6 respectively in the following (letters S and R stand for slow and rapid, respectively). On the one hand, the SPS material obtained by the atomisation at TLS of electrodes GFE1 will be used for mechanical tests (section 5). On the other hand, electrodes, powders and SPS billets from GFE2 will be used for microstructural and chemical analyses, to take advantage of the controlled atomization at HZG.

The SPS densifications of the EIGA powders were performed on the Dr Sinter Sumitomo 2080 apparatus (Sumitomo Coal Ming Co. Japan) implemented in the "*Plateforme Nationale de Frittage Flash /CNRS*" in Toulouse, France. The usual SPS cycle presented in details elsewhere [11] was used. The thermal cycle resulting from the application of a pulsed direct current consists of a temperature ramp at a rate of 100 K/min followed by a temperature plateau of

2 min at dwell temperature. A load corresponding usually to 50 MPa is applied at the beginning of the temperature ramp. At the end of the plateau, both current and load are switched off. Consistently with the high aluminium contents of the materials, the dwell temperatures used were relatively high, 1415°C and 1375°C for the GFE1 and GFE2 electrodes, respectively (these temperatures are the true temperatures of the material, i.e. the measured temperatures augmented by 60 K [11]).

The microstructures are mainly analysed by scanning electron microscopy (SEM) in back scattered electron imaging (BSE) mode, so that the origin of the contrast is related to the local chemical composition of the material: the larger the atomic number, the brighter the image. The measurements of the chemical compositions were performed at various scale. At a macroscopic scale (~ $1cm^3$ of material), ICP (Inductively Coupled Plasma) and IGA (Instrumental Gas Analysis) were used for the quantification of major and minor elements, respectively. Local chemical analyses of various elements were performed by SEM-EDX on the electrodes, powder particles and SPS samples. Each reported data represents an average of at least 10 local measurements. The experimental uncertainty on these EDX measurements is considered to be of the order of a few tenth of at. %. The SEM-EDX measurements were performed on areas of a few hundred square micrometers or locally using a SEM equipped with a field emission gun (FEG). In the following, our purpose is to focus on the three major alloying elements: Ti, Al and W, since the distribution of the other elements remain relatively stable at all stages of the production route.

Tensile tests were performed at a constant strain rate of 10^{-4} s^{-1} at room temperature (CEMES) and 800°C (ONERA).

3. Materials after the three successive steps of the processing

3.1. Electrodes

Fig. 2a shows the macrostructure of one electrode which is composed of columnar grains having a radial growth from the surface in contact with the cold mold, and an equiaxed structure in the centre area, the size of which tends to increase with the distance from the tip of the electrode. Such a microstructure is typical for cast TiAl alloys, both for peritectic [10] or β-solidified [12] alloys.

The chemical composition has been measured by ICP and IGA at six different locations along the length of the electrode (marked L1 to L6 in Fig. 2 a). It is found to be quite homogeneous all along the electrode length (Fig. 3). Figs. 2 b to e show the microstructure variations along a radius, from the centre to surface. Along the radius, a dendritic microstructure is observed whatever the equiaxed or columnar microstructure. From the centre to the surface, a decrease in the dendrite size is noticed. The chemical composition at these four locations has been measured by EDX-SEM, integrating the whole area shown in the micrographs. The results (Tab. 2) indicate that tungsten is homogeneously distributed in the radial direction as well as along the longitudinal axis. However, a slight but significant depletion in titanium is measured at the edge of the electrode.

Tab. 2. *Chemical compositions at the four locations along the radius shown in Fig. 2.*

	Ti	Al	W
Location (b) – Centre	48.6	48.6	2.0
Location (c) – Intermediate 1	48.6	48.7	1.9
Location (d) – Intermediate 2	48.5	48.8	1.9
Location (e) – Edge	47.6	49.6	1.9

3.2. Powder particles

Fig. 4 shows the powder particles for batches BR2 and BS5 obtained with the GFE2 electrode. Generally, the particles are spherical with a small number of satellites (Fig. 4 a and b). Their microstructure is made of a dendritic microstructure (Fig. 4 d). Such a dendritic microstructure is commonly observed in gas atomised TiAl powders and contains a large fraction of out-equilibrium α/α_2 phase [8,13,14]. The microstructure exhibits some bright features, the size of which being about 20 µm (Fig. 4 c). These bright features show well-defined contours, often bordered by a grey band (Fig. 4 c). Such bright features are not present in every particles but if present, several of them could generally be observed in a single particle.

These micrographs seem to show that the number of bright features is higher in the powder atomised at a high feeding rate. To quantify this point, an image analysis post-processing method has been applied using the ImageJ software, as illustrated in Fig. 4 e to h. The particles are delimited by image thresholding (Fig. 4 f) and the ones containing bright features are manually isolated (Fig. 4 g). The surface fraction of the bright areas is then measured by thresholding and counting the black pixels (Fig. 4 h). Results obtained for batches BR2 and BS5 are given in Tab. 3. It confirms that the number and surface fraction of bright features are approximately two times higher in the powder atomised at high feeding rate compared to the lower one.

Tab. 3. *Measurements of the bright surfaces in batches BR2 and BS5 of particles atomised from electrode GFE2.*

	Particle numbers (%)	Surface fraction (%)
BL5 - feeding rate: 16 kg/hour	35	5.4
BR2 - feeding rate: 45 kg/hour	65	11

3.3. SPS material

Fig. 5 a shows the microstructure of the sample obtained with the powder batch BL3 (low feeding rate: 16 kg/hour), to be compared to that displayed in Fig. 1 b (batch BR2 – high feeding

rate: 45 kg/hour). Similar microstructures were observed with the four other batches (not reproduced here). All these observations indicate a higher density of bright features in the SPS material obtained with the powders atomised at high feeding rate. To quantify this point, the surface fraction of these bright features were also measured by image processing using the ImageJ software. To achieve better statistics, measurements have been made at five positions for each sample, at the centre of the sample and at four mid-radius position at 90° from each other. These results are summarized in Tab. 4 and confirm a density of bright features about three times higher in samples densified with the powder atomised at high feeding rate. The relatively low value of the standard deviation indicates a homogeneous distribution of bright zones in the SPS material. Fig. 5 c shows at a large magnification some heterogeneities in the SPS material obtained after densification of powders from batch BS5. It appears that several bright features are concentrated in rather circular arrangements, which is consistent with the fact that these features are issued from former powder particles. Such bright features possess diffuse borders and seem to be connected when originating from the same particle. The microstructure is thus composed of bright zones issued from some former particles and being immersed in a homogeneous near-lamellar microstructure.

With regard to the chemical composition of the SPS material, for the GFE2 alloy, Fig. 3 compares the composition of this material with that of the six samples taken from the electrode. Little change is observed, except for an increase in oxygen content to 1200 ppm.

Tab. 4. Surface fraction of bright areas in the SPS billets obtained by the densification of the six batches of powders.

Batch	BS1	BR2	BS3	BR4	BS5	BR6
Surface fraction	1.2	13.8	4.6	16.7	6.1	11.2
Standard deviation	0.54	0.94	0.34	1.54	0.42	1.14

4. Microstructures and local chemical analyses

Fig. 6 displays the microstructures of the electrodes, powder particles and SPS materials at a higher magnification. Chemical measurements were carried out in the areas indicated by the color marks.

The microstructure of the electrode (Fig. 6 a) consists of dendritic cores surrounded by interdendritic areas. It is similar to that investigated in the cast W and Re containing alloys by Grange *et al.* [12]. The left part of the micrograph shows some dendritic cores which contain β phase skeletons highlighted in white, with a local measured W content in the order of 8 at. % (data in brown). The presence of this highly β-stabilizing element tends to retain this network of dendritic cores at room temperature which are enriched in W. These results are consistent with predictions about the phase constitution of the alloy based on CALPHAD calculations. Indeed, these calculations predict enrichment of W in a bcc phase which is below 8% phase fraction even for a W content of 8 at.%. The other phases found are γ, α_2 and β/β_0 as established for TiAl alloys. In the areas away from the dendritic cores and in the interdendritic channels, the W content is in the order of 1.2 at. % and 0.8 at. %, respectively (data in black - right part of Fig. 6 a).

In the powder particles (Fig. 6 b), away from the W concentration a non equilibrium dendritic microstructure with a large amount of α/α_2 phase is observed as usual in EIGA TiAl powders [15]. Concerning the bright features, as indicated by the EBSD insert in Fig. 6 b, the brighter zones (yellow in the EBSD map) are of β/β_0 phase and contain an amount of about 3 at. % of W (data in red in Fig. 6 b). The less bright peripheral zones are of α_2 phase (purple in the EBSD map).

In the SPS material (Fig. 6 c), the bright features appear to be located in any part of the microstructure, independently from lamellar colonies or γ borders which are surrounding these colonies and from the locally present phases.

Now focussing on the W content, using a magnification roughly at the particle size scale for both SPS sample and powder particles (Fig. 6 b and c - data in green and orange), the W contents is in the order of 2 at. %. There slight increase of W (2.2 at. %- green zone - Fig. 6 c) in the SPS sample in the surrounding of the bright features is within our experimental uncertainty. Besides, for magnifications at the scale of the bright features (~20 µm), some fairly clear correspondences can be pointed out. The bright features have about 3 at. % of W in both the particles and the SPS sample (data in red - Fig. 6 b and c). Moreover, when considering as a dendritic core 20 µm in size around the skeletons, the same W content of about 3 at. % is found (data in red - Fig. 6 a).

The zones between these bright features in the dendritic structure of particles and in the lamellar colonies of the SPS sample contain slightly less than 2.0 at. % of W in both cases (data in blue - Fig. 6 b and c). This indicates that a similar W content is obtained, everywhere microstructural heterogeneities are not present.

5. Mechanical properties

The effect of these chemical heterogeneities on the mechanical properties were evaluated by performing tensile tests using the SPS alloy processed with the powder atomised from the GFE1 electrode. Its microstructure (Fig. 7) is similar to those already presented with batches of powders atomised at low feeding rate (Fig. 5 c).

In Figure 8 a and b, tensile curves of this GFE1-IRIS alloy at room temperature and at 800°C are compared with those obtained with the heterogeneity-free TGA-SPS-IRIS alloy [3]. In Fig. 8 a, the colour curves (red, blue and green) show tests which were carried out on specimens extracted from three GFE1-IRIS pellets densified under the same conditions. For the sake of clarity, these curves were offset by 0.5%. This graph shows the high reproducibility of the mechanical behaviour of the GFE1-IRIS densified alloy despite the presence of chemical

heterogeneities. Such reproducibility has already been measured in several TiAl alloys densified by SPS with TGA powders [2,3]. Comparison with the tensile behaviour of the TGA-SPS-IRIS alloy (black curve) shows a slight drop in strength and ductility. From the curves in Figure 7 b at 800°C, a slight reduction in strength coupled with a sharp decrease in plastic elongation are observed.

In summary, these results underline a relatively small influence of the heterogeneities on the mechanical strength of the TiAl IRIS-SPS alloy, in particular for the dimensioning properties for applications, such as high temperature strength and room-temperature ductility.

6. Discussion

In this work, the microstructures and the local chemical compositions of the IRIS alloy obtained after the three successive steps (centrifugal casting, atomisation and SPS densification) have been studied. Local enrichments of W due to segregation have been found after each steps. In the atomised bar, the melting appears insufficient to homogenise the alloyed concentration of W. The atomisation step constraints these heterogeneities in some particles. The bright features observed in the powder after atomisation and in the SPS material after densification exhibit several similarities: (i) their average W content is close to 3 at. %; (ii) their characteristic dimension is about 20 µm, and (iii) in general, several of them are close to each other. Such similarities can be extended to the dendritic cores of the electrode considering they have similar size. These observations thus indicate that the W enrichment of the SPS samples originate from the W enrichment from the powder particles, themselves derived from the segregations observed in the dendritic cores of the electrode.

An attempt to explain the mechanism of the formation of those W enrichments is given below. Starting from the electrode, as described in the W and Re containing G4 alloy [12] which similarly to IRIS solidifies through the β phase field, β skeletons result from the retention of

primary β phase grown from liquid during the first solidification. Note that in these skeletons, the aluminium content is very low, which confirms that they are issued from the first solidified layers according to the description of Grange *et al.* [12]. They are thus probably not avoidable during solidification, even at very low solidification rate. In the electrode, these skeletons form interlinked networks, which explains the formation of several connected bright features in the particles.

During the EIGA atomisation, these first solidified parts of the electrode probably fall in the nozzle before a complete melting, thus leading to numerous and connected bright features in the particles. This results in homogeneous bright features in the particles with pronounced boundaries. In these zones corresponding to the dendritic cores, during the EIGA process the expansion of the β phase occurs, accompanied by a local homogenisation of the W content. Their periphery is constituted of α phase consistently with a lower W content.

The increasing number of W enrichments with increasing feeding rate during atomisation, which reduces the time available to fully melt potential W-rich segregation in molten TiAl seems to support this interpretation. A FEM simulation of the electrode during melting was realised using Freefem++ software. The model was simplified to an axisymmetric problem and only thermal equilibrium was calculated. Boundary conditions were as follows:

- A Neumann condition on all the free surface modelling the heat exchange with the Ar-shielding atmosphere in the atomisation tower. The external temperature was set to 250°C and a heat transfer coefficient of 200 W/(m^2*K) was used;
- A Dirichlet condition was applied on the conical-melted surface of the electrode, representing the coupling with the induction coil. A constant temperature of 1800°C was applied.

The speed was varied from $9.8*10^{-4}$ m/s (16 kg/h) to $2.8*10^{-3}$ m/s (45 kg/h), which corresponds to the melting of the electrode 20 mm in diameter. Figures 9 a and b represent the temperature

field obtained in both cases. It appears that the higher the feeding rate, the shorter the melted area. Using the time equivalent, the temperature profile for a solid fraction at the centre of the electrode with time is given in figure 9 c.

For simplification, if full melting of the material is reached for temperature higher than 1500°C, the residence time of potential W-skeleton in molten TiAl is 3 s and 11 s for 45 and 16 kg/hour feeding rates, respectively. Clearly, the present results indicate that the residence time should be higher than 11 s to completely dissolve the W-skeleton and thus improve the homogeneity of the powder. This is consistent with results obtained on TGA, PIGA and VIGA powders where the material is fully molten and homogenised before atomisation, eliminating the first solidified areas and allowing more homogeneous powders.

During the SPS cycle, peripheral diffusion occurs resulting in diffuse contours for the bright areas in the SPS samples, but with an unchanged W content due to its low mobility in solid state.

Regarding areas without any W segregations, i.e. where the alloy was fully molten during the EIGA process, the dendritic structure of the particles with a high proportion of out-of-equilibrium hexagonal phase leads to the formation of a quasi-lamellar structure in the final material, which is composed of lamellar colonies and γ borders [17]. In these zones free of heterogeneities, measurements of aluminium and titanium contents lead to fluctuating values, the significance of which is still under debate. Among the three stages of the processing route, it is difficult to explain such variations which may be within our measurement uncertainty. However, these variations may also result from local heterogeneities in the initial electrode depending on the position of the atomised material and/or relative to the dendritic microstructure, since little species migration is expected during the atomisation and the densification cycles.

7. Summary

In this work, the present authors have gathered to understand why an IRIS alloy densified by SPS with a powder atomised by the EIGA process exhibits chemical heterogeneities in the form of tungsten segregations. By tracing back these heterogeneities throughout the manufacturing process (centrifugal casting, atomisation and SPS densification), it was shown that these heterogeneities originated from the retention of the primary β phase in the dendritic cores present in the initial electrode. All along the process, the diffusion of tungsten atoms is too limited to achieve complete homogenisation of the final material.

Despite a dramatic appearance in scanning electron micrographs taken with backscattered electrons, the local W enrichment is only 1 at. %. in these heterogeneous zones, whereas in the rest of the SPS material, the W content is maintained at a little less than 2 at. %. This is the reason why mechanical properties at room and high temperatures have been found to be only slightly affected by the presence of these heterogeneities.

Acknowledgements

This study has been (partially) supported through the grant NanoX n° ANR-17-EURE-0009 in the framework of the « Programme des Investissements d'Avenir" through the project "ALTIAUTO".

References

[1] F. Appel, J. Paul, M. Oehring: *Gamma Titanium Aluminides : Science and Technology, © Wiley-VCH Verlag GmbH &Co. KGaA,* 2011.

[2] A. Couret, J. P. Monchoux, M. Thomas, T. Voisin, Procédé de fabrication d'une pièce en alliage TiA, Patent WO2014199082 A, (2013).

[3] T. Voisin, J. P. Monchoux, C. Deshayes, M. Thomas, A. Couret, Mechanical properties of the IRIS TiAl alloy, DOI: 10.1007/s11661-016-3801-3, Metallurgical and Materials Transactions 47A, 12 (2016) 6097-6108.

[4] M.P. Bacos, S. Ceccati, J.P. Monchoux, C. Davoine, T. Gheno, C. Rio, A. Morel, J.S. Merot, F. Fossard, M. Thomas, Oxidation Behavior of a Spark Plasma Sintered Ti-48Al-2W-0.1B Alloy at 800 °C, DOI: 10.1007/s11085-020-09973-8, OXIDATION OF METALS, 93 (2020) 587-600.

[5] A. Couret, D. Reyes, M. Thomas, N. Ratel-Ramond, C. Deshaeyes, J. P. Monchoux, Effect of long-term ageing on the properties of the W-containing IRIS-TiAl alloy, DOI: 10.1016/j.actamat.2020.07.061, Acta Materialia 199 (2020) 169-180.

[6] A. Couret, J. P. Monchoux, D. Caillard, On the high creep strength of the W containing IRIS-TiAl alloy at 850 °C, DOI: 10.1016/j.actamat.2019.09.056, Acta Mat., 181 (2019) 331-341.

[7] C.F. Yolton, Y.W. Kim, U. Habel, Powder metallurgy processing of gamma titanium aluminide, GAMMA TITANIUM ALUMINIDES 2003 Edited by:Kim, YW; Clemens, H; Rosenberger, AH, (2003) 233-240.

[8] R. Gerling, H. Clemens, FP. Schimansky, Power metallurgical processing of intermetallic gamma titanium aluminides, DOI: 10.1002/adem.200310559, Advanced Engineering Materials 2004; 6: 23.

[9] J.J. Dunkley, Metalpowder atomisation methods for modern manufacturing, DOI: 10.1595/205651319X15583434137356, JOHNSON MATTHEY TECHNOLOGY REVIEW, 63 (2019), 226-232.

[10] V. Güther, M. Allen, J. Klose, H. Clemens, Metallurgical processing of titanium aluminides on industrial scale, DOI: 10.1016/j.intermet.2018.09.006, Intermetallics, 103 (2018) 12-22.

[11] T. Voisin, L. Durand, N. Karnatak, S. Le Gallet, M. Thomas, Y. Le Berre, J.F. Castagné, A. Couret, Temperature control during Spark Plasma Sintering and application to up-scaling and complex shaping, DOI: 10.1016/j.jmatprotec.2012.09.023 Journal of Materials and Processing 213 (2012) 269-278.

[12] M. Grange, J.L. Raviart, M. Thomas, Influence of microstructure on tensile and creep properties of a new castable TiAl-based alloy, DOI: 10.1007/s11661-004-0157-x, Metallurgical and Materials Transactions 35A, 7 (2016) 2087-2102.

[13] U. Habel, C.F. Yolton, J.H. Moll, Gas atomized gamma-titanium aluminide based alloys - Processing, microstructure and mechanical properties, Gamma Titanium Aluminides, TMS, Warrendale, (1999) 301-308.

[14] H. Jabbar, J.P. Monchoux, M. Thomas, A. Couret, Microstructures and deformation mechanisms of a G4 TiAl alloy produced by spark plasma sintering, DOI: 10.1016/j.actamat.2011.09.001, Acta Materialia 59 (2011) 7574-7585.

[15] H. Jabbar, A. Couret, L. Durand, J.P. Monchoux, Identification of microstructural mechanisms during densification of a TiAl alloy by spark plasma sintering, Journal of alloys and compounds, 10.1016/j.jallcom.2011.08.008, 509, 9826-9835, 2011

[16] A. Couret, G. Molénat, J. Galy, M. Thomas M., Microstructures and mechanical properties of TiAl alloys consolidated by spark plasma sintering, DOI: 10.1016/j.intermet.2008.06.015, Intermetallics 16 (2008) 1134-1141.

[17] T. Voisin, J. P. Monchoux, M. Perrut, A. Couret A, Obtaining of a fine near-lamellar microstructure in TiAl alloys by Spark Plasma Sintering, DOI: 10.1016/j.intermet.2016.01.003, Intermetallics, 71 (2016) 88-97.

Figure captions

Fig. 1. Microstructures of the TGA-SPS-IRIS (a) and GFE2-SPS-IRIS (b) alloys densified by SPS, using the same processing parameters. The micrographs were recorded in the same microscope using the same conditions.

Fig. 2. Macrostructure (a) of the longitudinally cut symmetric area of the electrode and microstructures (b to e) along a radius. L1 to L6 mark the positions at which the chemical measurements were performed.

Fig. 3. Measurements of the chemical composition of the electrode at the six positions, L1 to L6, as well as that of the SPS material for comparison.

Fig. 4. SEM and quantitative study of the powder particles. (a) and (b) micrographs of particles of batches BR2 and BS5 at a low magnification (GFE2 electrodes); (c) and (d) particles with and without bright features at a higher magnification and (e) to (h) illustration of the measurement method of the number of particles containing bright features and of the surface fraction covered by the bright areas.

Fig. 5. SPS material. (a) microstructure at low magnification (batch BS3); (b) binarized image of (a), and (c) microstructure at high magnification (batch BS5).

Fig. 6. Local chemical analyses by SEM-EDX of various elements of the microstructure of electrodes (a), powder particles (b) and SPS materials (c). All the materials were obtained with a GFE2 electrode. The insert of (b) shows a EBSD map of a bright zone.

Fig. 7. Microstructures of the GFE1-EIGA-SPS-IRIS alloy at a dwell temperature of 1365°C.

Fig. 8. Tensile curves at room temperature (a) and 800°C (b), showing the true stress (σ) as function of the plastic strain (ε). Color curves correspond to the GFE1-EIGA-SPS-IRIS alloy and black ones to the TGA-SPS-IRIS alloy.

Fig. 9. FEM modelling of the electrode during the atomisation. (a) and (b) temperature distributions in the molten electrode at 16 kg/h and 45 kg/h, respectively; (c) evolution of the temperature with time for a solid part at the centre of the electrode.

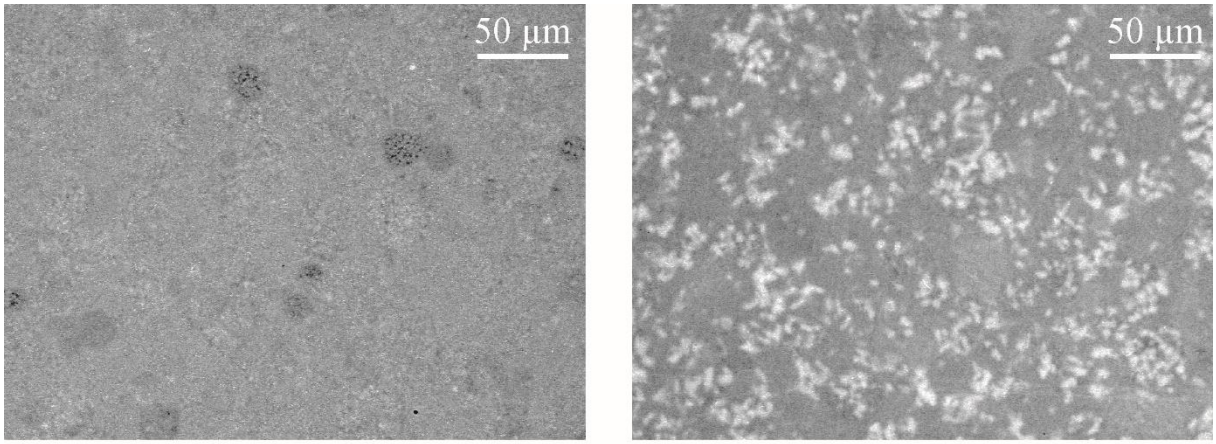

Fig. 1. Microstructures of the TGA-SPS-IRIS (a) and EIGA-SPS IRIS (b) alloys densified by SPS, using the same processing parameters. The micrographs were recorded in the same microscope using the same conditions.

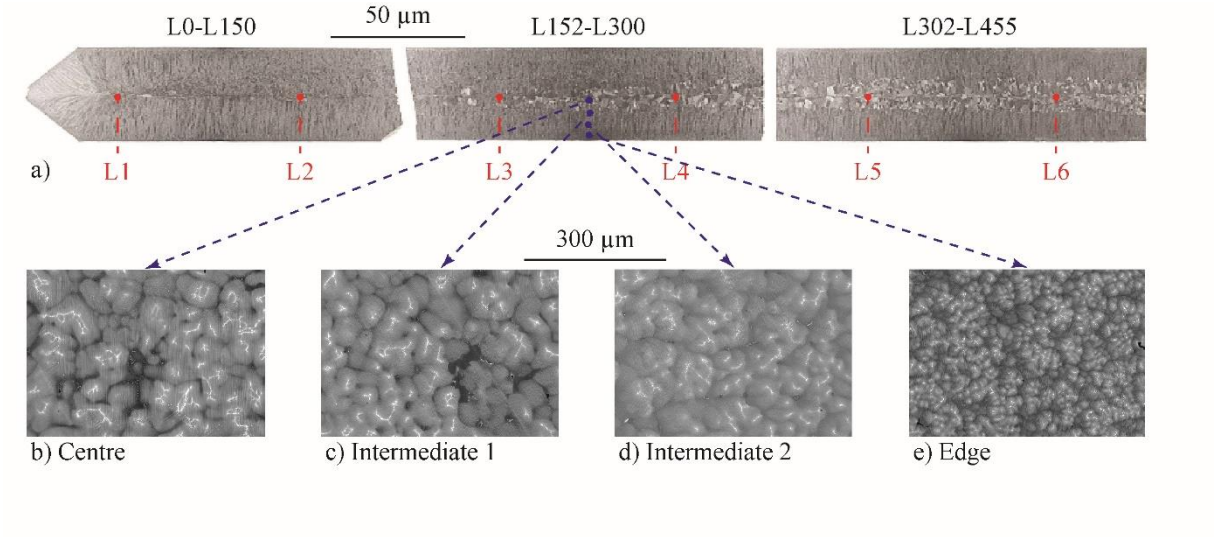

Fig. 2. Macrostructure (a) of the longitudinally cut symmetric area of the ingot and microstructures (b to e) along a radius. L1 to L6 mark the positions at which the chemical measurements were performed.

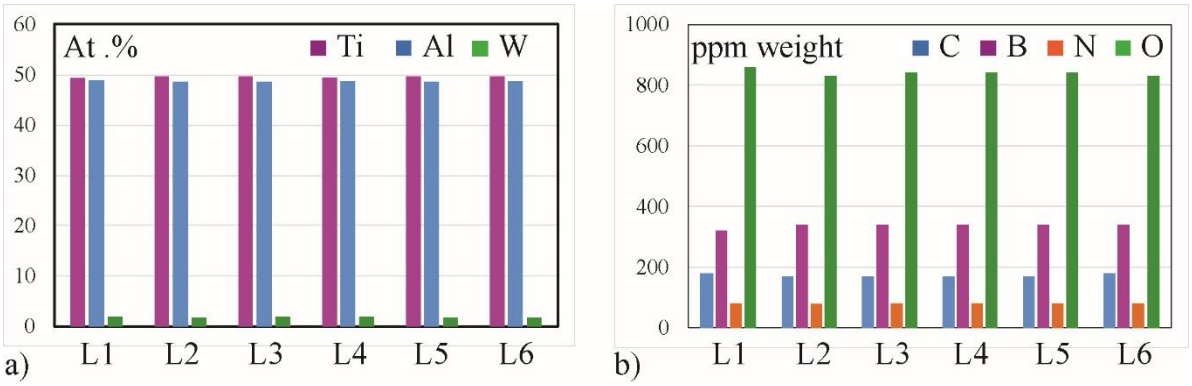

Fig. 3. Measurements of the chemical position of the ingot at the six positions, L1 to L6.

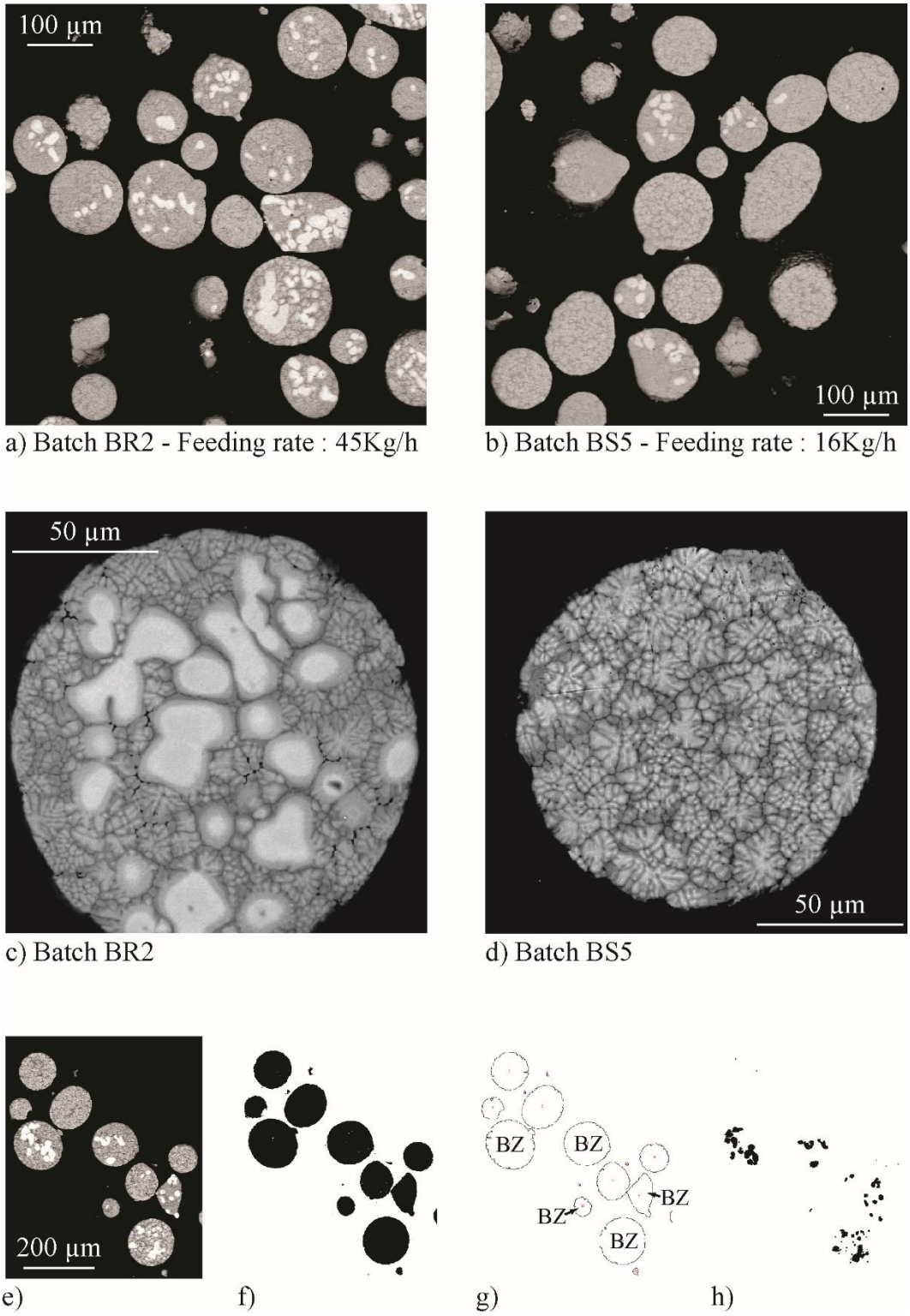

Fig. 4. SEM and quantitative study of the powder particles. (a) and (b) micrographs of particles of batches BR2 and BS5 at a low magnification; (c) and (d) particles with and without bright zones at a higher magnification and (e) to (h) illustration of the quantitative measurements of the number of particles containing bright zones and of the surface fraction covered by the bright zones.

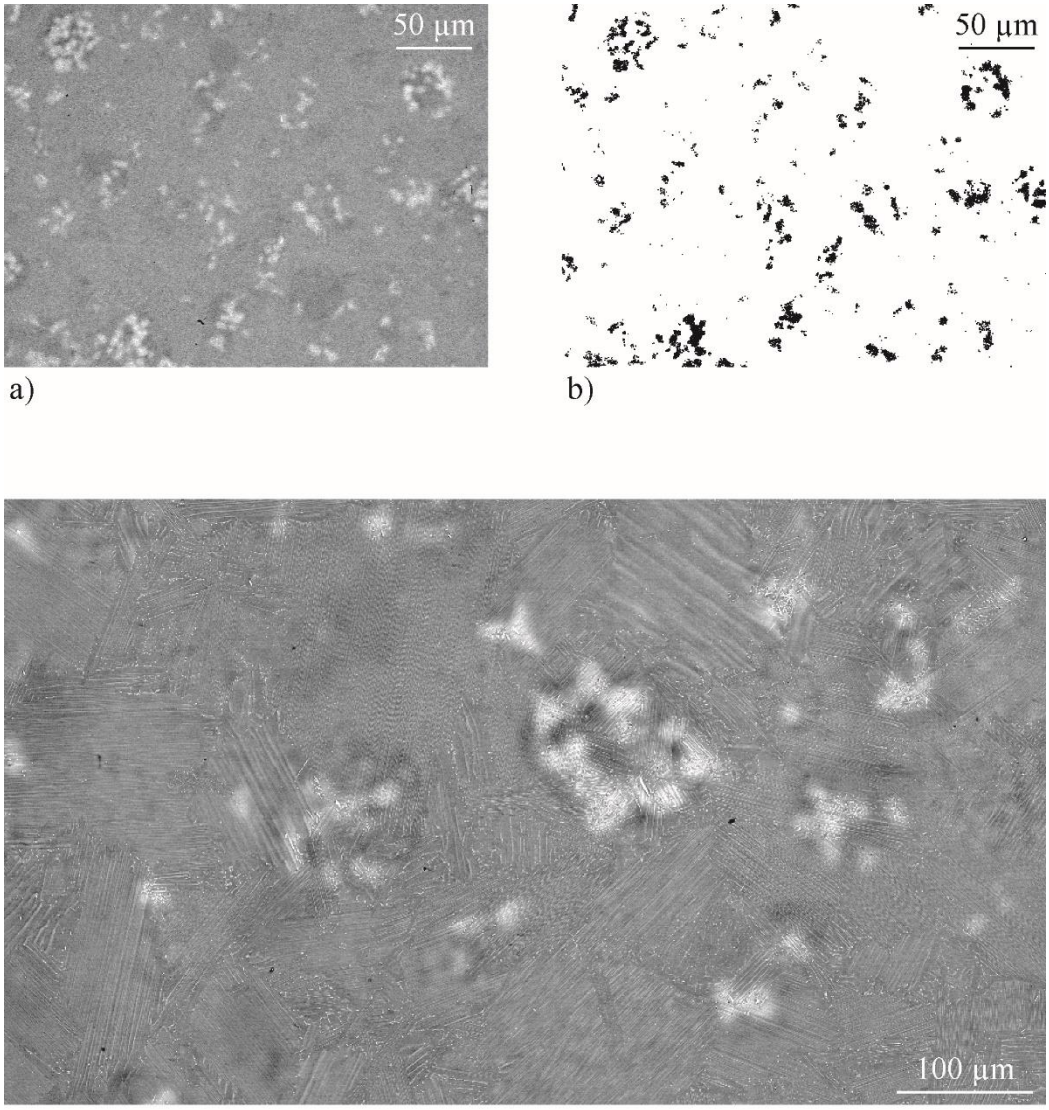

Fig. 5. SPS material. (a) microstructure at low magnification (batch BS3); (b) binarized image of (a) and (c) microstructure at high magnification (batch BS5).

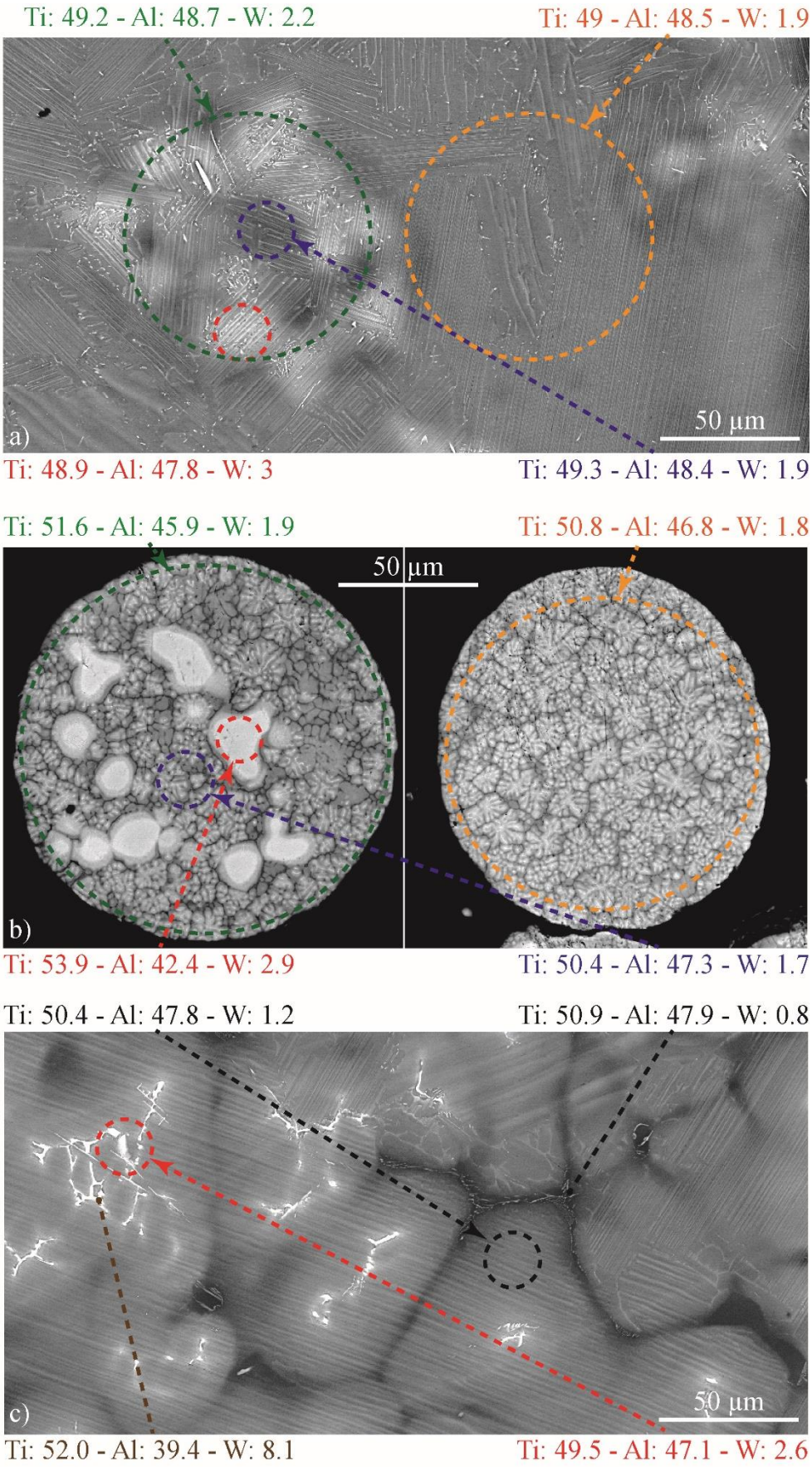

Fig. 6. Local chemical analyses by SEM-EDX of various elements of the microstructure of SPS materials (a), powder particles (b) and ingot (c).

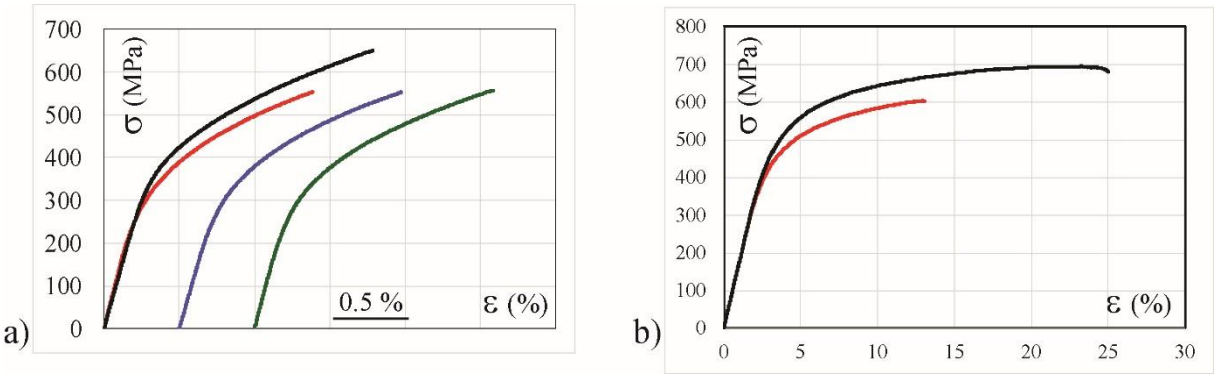

Fig. 7. Tensile curves at room temperature (a) and 800°C (b). Color curves correspond to the EIGA-SPS-IRIS-2 alloy and black ones to the TGA-SPS-IRIS alloy.

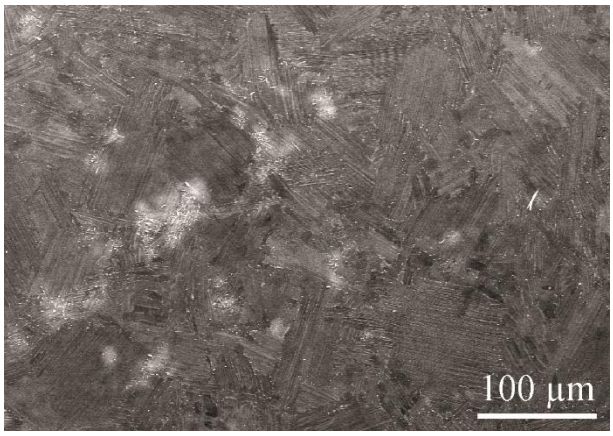

Fig. 8. Microstructures of the EIGA-SPS-IRIS-2 alloy at a dwell temperature of 1365°C.

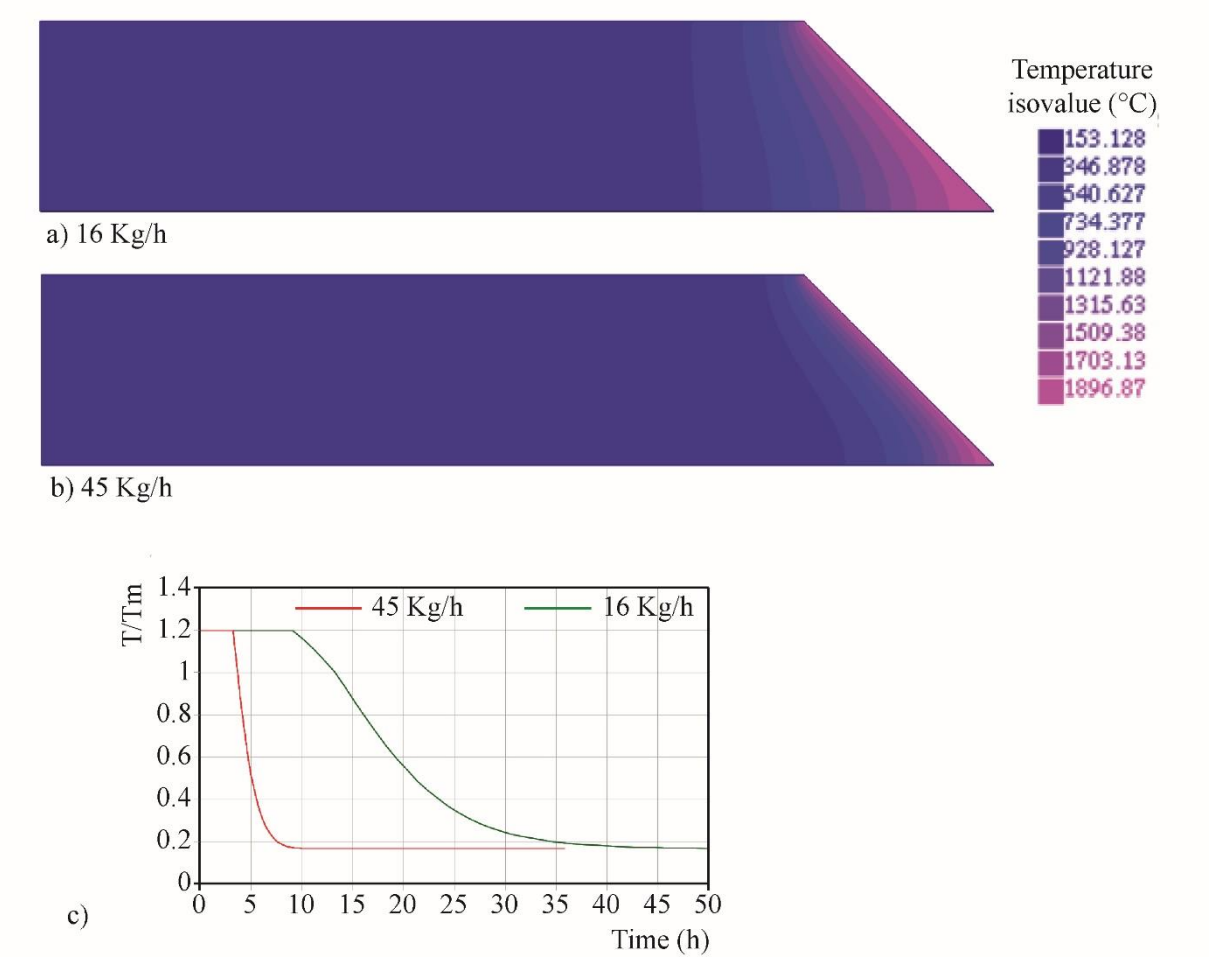

Fig. 9. FEM modelling of the electrode during the atomisation. (a) and (b) temperature distributions in the melted electrode at 16 kg/h and 45 kg/h, respectively; (c) evolution of the temperature with time for a solid particle at the centre of the electrode.